
Size Generalization of Graph Neural Networks on Biological Data: Insights and Practices from the Spectral Perspective

Gaotang Li¹ Danai Koutra¹ Yujun Yan²

Abstract

We investigate size-induced distribution shifts in graphs and assess their impact on the ability of graph neural networks (GNNs) to generalize to larger graphs relative to the training data. Existing literature presents conflicting conclusions on GNNs’ size generalizability, primarily due to disparities in application domains and underlying assumptions concerning size-induced distribution shifts. Motivated by this, we take a data-driven approach: we focus on real biological datasets and seek to characterize the types of size-induced distribution shifts. Diverging from prior approaches, we adopt a spectral perspective and identify that spectrum differences induced by size are related to differences in subgraph patterns (e.g., average cycle lengths). While previous studies have identified that the inability of GNNs in capturing subgraph information negatively impacts their in-distribution generalization, our findings further show that this decline is more pronounced when evaluating on larger test graphs not encountered during training. Based on these spectral insights, we introduce a simple yet effective model-agnostic strategy, which makes GNNs aware of these important subgraph patterns to enhance their size generalizability. Our empirical results reveal that our proposed size-insensitive attention strategy substantially enhances graph classification performance on large test graphs, which are 2-10 times larger than the training graphs, resulting in an improvement in F_1 scores by up to 8%.

1. Introduction

Graph neural networks (GNNs) (Kipf & Welling, 2017; Veličković et al., 2018; Hamilton et al., 2017; Zhang et al., 2018; Yan et al., 2019; Lee et al., 2018) have gained widespread popularity in graph classification tasks owing

¹University of Michigan, Ann Arbor ²Dartmouth College. Correspondence to: Gaotang Li <gaotang@umich.edu>.

Preprint.

to their outstanding performance. Though most GNNs can process graphs of varying sizes, it remains under-explored whether they can generalize to graphs larger than those encountered during training (size generalizability). Size generalization in GNNs holds significant importance across multiple domains. For instance, in graph algorithmic reasoning (Yan et al., 2020; Veličković et al., 2020), GNNs are expected to learn complex algorithms from small examples and generalize that reasoning to larger graphs, as obtaining exact solutions for larger graphs is challenging. In the realm of biology, datasets exhibit a wide range of graph sizes, spanning from small molecules to large compounds. Evaluating whether learned knowledge is influenced by graph size is crucial, as size-dependent information may potentially have a detrimental impact on performance when employing pre-training strategies (Hu et al., 2020c).

Existing literature presents conflicting conclusions on GNNs’ size generalizability. On one hand, several studies (Levie et al., 2021; Xu et al., 2021; Sanchez-Gonzalez et al., 2020) have provided support for the ability of GNNs to effectively generalize across varying sizes. For instance, a theoretical study (Levie et al., 2021) established that spectral GNNs exhibit robust transferability between graphs with different sizes and topologies, provided that these graphs discretize the same underlying space in some generic sense. Other works further provided empirical evidence supporting the strong size generalizability of GNNs in the domains of algorithmic task learning (Xu et al., 2021) and physics simulations (Sanchez-Gonzalez et al., 2020). On the other hand, several studies (Yehudai et al., 2021; Buffelli et al., 2022; Bevilacqua et al., 2021) have observed performance degradation when a size shift exists between the training and test data. For instance, a recent work (Yehudai et al., 2021) showed theoretically and empirically that the difference in d-patterns between small and large graphs contributes to this performance decline. However, we find that d-patterns cannot effectively capture variations in cycle statistics (Appendix K), a critical factor for the generalization of GNNs to larger biological graphs, as highlighted in this paper. There have also been proposals of novel models (Bevilacqua et al., 2021) and regularization techniques (Buffelli et al., 2022) to enhance the size generalizability of GNNs. These conflicts mainly arise from disparities in application domains and un-

derlying assumptions concerning size-induced distribution shifts.

Motivated by these conflicts, we take a data-driven approach: we focus on real biological datasets and seek to characterize the types of size-induced distribution shifts. This characterization provides valuable insights into the size generalizability of GNNs. Specifically, we adopt a spectral perspective and identify the connections between the spectrum differences induced by varying graph sizes and the differences in subgraph patterns, particularly cycles. We find that breaking cycles in graphs amplifies the spectrum difference between smaller and larger graphs, whereas extending cycle lengths in smaller graphs to align with those in larger graphs reduces this difference. Furthermore, we observe that conventional GNNs struggle to generalize effectively without explicit cycle information, leading to performance degradation on larger graphs. While prior research has emphasized GNNs’ limitations in counting and recognizing cycles (Chen et al., 2020) within in-distribution generalization, this paper systematically explores their impact in out-of-distribution scenarios, specifically focusing on size generalizability. To address the above issues, we introduce a Size-Insensitive Attention (SIA) approach to enhance any GNNs. This is achieved by encoding cycle information into the feature representations and leveraging them within a size-insensitive attention mechanism to guide the learning process. To substantiate the utility of cycle information, we examine the performance of two additional simple baselines that also incorporate cycle information. Empirical evidence confirms that integrating cycle information indeed aids in GNN size generalization, and our proposed SIA strategy substantially boosts model performance on large test sets and surpasses the state-of-the-art models by a large margin.

In sum, our paper makes the following contributions:

- **New Observations.** We characterize the types of distribution shifts caused by various graph sizes in biological networks, offering insights for designing a size-agnostic GNN.
- **Spectral Analysis.** Unlike prior work, we leverage spectral analysis to deepen our understanding of the size generalizability of GNNs.
- **Effective Model-agnostic Strategy.** To make GNNs aware of important size-related subgraph patterns (e.g., average cycle lengths), we propose a size-insensitive attention that can seamlessly integrate with various architectures. Experimental findings indicate that our method significantly enhances the size generalizability of GNNs and outperforms the baselines by a large margin.

2. Notations and Preliminaries

In this section, we begin by introducing the notations and definitions used throughout the paper. Next, we provide an

introduction to the fundamentals of GNNs.

2.1. Notations & Definitions

Let $\mathcal{G}(\mathcal{V}, \mathcal{E})$ be an undirected and unweighted graph with N nodes, where \mathcal{V} denotes the node set, and \mathcal{E} denotes the edge set. The neighborhood of a node v_i is defined as the set of all nodes that connect to v_i : $\mathcal{N}_i = \{v_j | (v_j, v_i) \in \mathcal{E}\}$. The graph is represented by its adjacency matrix $\mathbf{A} \in \mathbb{R}^{N \times N}$, and it has a degree matrix \mathbf{D} , where the i th diagonal element d_i corresponds to the degree of node v_i .

Cycle basis. An important concept we use to study cycles is *cycle basis* (Sysło, 1979). A cycle basis is defined as the smallest set of cycles where any cycle in the graph can be expressed as a sum of cycles from this basis, similar to the concept of a basis in vector spaces. Here, the summation of cycles is defined as “exclusive or” of the edges. We represent the cycle basis for a graph as \mathcal{C} and refer to the j th cycle in this cycle basis as \mathcal{C}_j . The cycle basis can be found using the algorithm CACM 491 (Paton, 1969).

2.2. Graph Learning Task

In this paper, we focus on the graph classification task, where each node v_i is associated with a feature vector $\mathbf{x}_i^{(0)}$, and the feature matrix $\mathbf{X}^{(0)}$ is constructed by arranging the node feature vectors as rows. When using a GNN for the graph classification task, we further denote the node representation matrix at the l -th layer as $\mathbf{X}^{(l)}$, and the representation of node v_i as $\mathbf{x}_i^{(l)}$.

Supervised Graph Classification. Each graph \mathcal{G}_i is associated with a label $y_i^{\mathcal{G}}$ sampled from a label set $\hat{\mathcal{L}}$. Given a subset of labeled graphs (from a label set $\hat{\mathcal{L}}$), the goal is to learn a mapping $f^{\mathcal{G}} : (\mathbf{A}, \mathbf{X}^{(0)})_i \mapsto y_i^{\mathcal{G}}$ between each graph \mathcal{G}_i and its ground truth label $y_i^{\mathcal{G}} \in \hat{\mathcal{L}}$. The graph classification loss is given by $L = \frac{1}{|\mathcal{G}_{\text{train}}|} \sum_{\mathcal{G}_i \in \mathcal{G}_{\text{train}}} \text{CrossEntropy}(\mathbf{x}^{\mathcal{G}_i}, y_i^{\mathcal{G}})$, where $\mathcal{G}_{\text{train}}$ is the training graph set and $\mathbf{x}^{\mathcal{G}_i}$ is the representation of graph \mathcal{G}_i .

Evaluation of Size Generalizability. Following prior work (Buffelli et al., 2022; Yehudai et al., 2021), we evaluate the size generalizability of GNNs by testing their classification performance on graphs whose sizes are larger than those in the train set. We obtain the small training graphs and large test graphs from the same dataset.

2.3. Graph Neural Networks

GNNs can be designed from either the spatial perspective or the spectral perspective. Despite the difference in the design perspectives, a recent work (Balcilar et al., 2021a) has shown that spectral GNNs and spatial GNNs are related and that spectral analysis of GNNs’ behavior can provide a complementary point of view to understand GNNs in general. Most spatial GNNs (Kipf & Welling, 2017; Xu et al., 2018; Veličković et al., 2018; Hamilton et al., 2017) use the

message passing framework (Gilmer et al., 2017), which consists of three steps: neighborhood propagation, message combination and global pooling. Spectral GNNs (Bo et al., 2021; Defferrard et al., 2016; Levie et al., 2018) utilize the spectral properties of a propagation matrix \mathbf{T} to perform the graph classification. The matrix \mathbf{T} is usually a function of the adjacency matrix \mathbf{A} , such as the normalized adjacency matrix $\mathbf{T} = (\mathbf{D} + \mathbf{I})^{-1/2}(\mathbf{A} + \mathbf{I})(\mathbf{D} + \mathbf{I})^{-1/2}$, or the normalized graph Laplacian matrix $\hat{\mathbf{L}}$. Since we consider an undirected graph with a real and symmetric adjacency matrix, the matrix \mathbf{T} is also real and symmetric. Then, we can perform the eigendecomposition on the propagation matrix \mathbf{T} : $\mathbf{T} = \mathbf{U}\mathbf{\Lambda}\mathbf{U}^T$, where \mathbf{U} is an orthogonal matrix whose columns \mathbf{U}_i are orthonormal and are the eigenvectors of \mathbf{T} , and $\mathbf{\Lambda}$ is a matrix whose diagonal elements are the eigenvalues of \mathbf{T} , sorted from large to small by their absolute values. The set of eigenvectors $\{\mathbf{U}_i\}$ form the orthonormal basis of \mathbb{R}^n . The goal of a spectral GNN is to learn a proper spectral filter: $f(\mathbf{\Lambda}) = c_0\mathbf{I} + c_1\mathbf{\Lambda} + c_2\mathbf{\Lambda}^2 + \dots + c_i\mathbf{\Lambda}^i + \dots$, where c_i are the learnable coefficients. The convolution at each layer can be viewed as or is equivalent to: $\mathbf{X}^{(l+1)} = \sigma(\mathbf{U}f(\mathbf{\Lambda})\mathbf{U}^T\mathbf{X}^{(l)}\mathbf{W}^{(l)})$, where $\mathbf{W}^{(l)}$ is a learnable weight matrix, and $\sigma(\cdot)$ is a nonlinear function (e.g., ReLU). The graph representation is obtained from the node representations at the last convolution layer: $\mathbf{x}^{\mathcal{G}} = \text{Pooling}(\{\mathbf{x}_i^{(\text{Last})}\})$, where the `Pooling` function is performed on the set of all the node representations, and it can be `Global_mean` or `Global_max` or other more complex pooling functions (Ying et al., 2018; Knyazev et al., 2019).

3. Spectral Analysis of Size-induced Distribution Shifts

In this section, we first show that the independence of the eigenvalue distribution of the propagation matrix \mathbf{T} from the graph size is the key to achieving size generalizability of GNNs (§ 3.1). Next, focusing on biologically data, we empirically verify that the eigenvalue distribution of the propagation matrix depends on the graph size (§ 3.2). Finally, we explore the subgraph patterns responsible for the spectral disparities between small and large graphs, unveiling two key findings in § 3.3:

- Breaking cycles in graphs amplifies the spectrum difference between smaller and larger graphs.
- Extending cycle lengths in smaller graphs to match larger ones reduces the spectrum difference.

3.1. Graph Spectrum and Size Generalizability of GNNs

To understand how GNNs generalize over graphs with different sizes, we examine the formulation of graph representations. In the context of spectral GNNs, graph representations rely on the eigenvalues of the propagation matrix. Consequently, the connection between graph representations and graph size reduces to the connection between the graph’s

Table 1. Average Wasserstein distance between graphs of ‘similar sizes’ and graphs of ‘different sizes’ based on **eigenvalue** distributions, respectively. The relative difference is computed by the difference of the Wasserstein distance normalized by the Wasserstein distance of similar graphs.

	BBBP	BACE	PROTEINS	NCI109	NCI1
Different Size	0.00566	0.00411	0.00765	0.00563	0.00566
Similar Size	0.00184	0.00149	0.00261	0.00215	0.00215
Relative Difference	208%	177%	193%	162%	164%

spectrum and its size. More formally, we theoretically show the following proposition in Appendix A.

Proposition 3.1. *When graphs of various sizes exhibit distinct eigenvalue distributions for the propagation matrix, the representations learned by spectral GNNs correlate with the graph size.*

The proposition suggests that for GNNs to achieve effective generalization to larger graphs, the disparity in the spectrum between small and large graphs should be small.

3.2. Size-related Spectrum Differences in Real Datasets

We now investigate how the eigenvalue distribution of the normalized adjacency matrix varies with graph size in real-world data. As indicated in Proposition 3.1, the spectrum discrepancy between small and large graphs affects the size generalizability of GNNs.

Datasets. We explore five pre-processed biological datasets (BBBP, BACE, NCI1, NCI109, and PROTEINS) from the Open Graph Benchmark (Hu et al., 2020b) and Tu-Dataset (Morris et al., 2020). More details about the datasets are provided in Appendix B.

Setup. Figure 1 illustrates the pairwise distances of the graphs arranged in ascending order of size, where the distances are calculated using the Wasserstein distance (Villani et al., 2009). We represent the graphs by their empirical distributions of the eigenvalues that are obtained from the normalized adjacency matrix as suggested in (Kipf & Welling, 2017): $\mathbf{T} = (\mathbf{D} + \mathbf{I})^{-1/2}(\mathbf{A} + \mathbf{I})(\mathbf{D} + \mathbf{I})^{-1/2}$. Using the normalized Laplacian matrix leads to similar observations. We note that the eigenvalues do not scale with the graph size, and they are bounded between $[-1, 1]$. Dark blue represents a small distance (high similarity) while light red represents a large distance (low similarity).

Results. As can be seen in the three subplots in Figure 1, there is a wide blue band along the diagonal, which indicates that graphs of similar size have more similar eigenvalue distributions than graphs of different sizes. This suggests a strong correlation between the eigenvalue distributions and the graph size. To verify the observation quantitatively, we compute the distance of graphs with ‘similar size’ and graphs of ‘different sizes’ in Table 1. For each graph, we consider the 20 most ‘similar graphs’ in terms of size, and

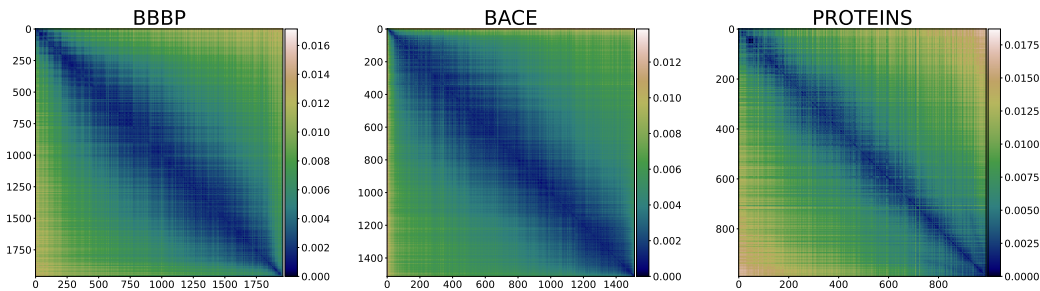


Figure 1. Pairwise graph distance of eigenvalue distributions: Graphs are sorted from small to large, and the (i,j)-th pixel in the plot represents the Wasserstein distance between the i-th and j-th graphs. Dark blue represents a small distance (high similarity), while light red represents a large distance (low similarity). We find that **eigenvalue distributions show a strong correlation with the graph size**.

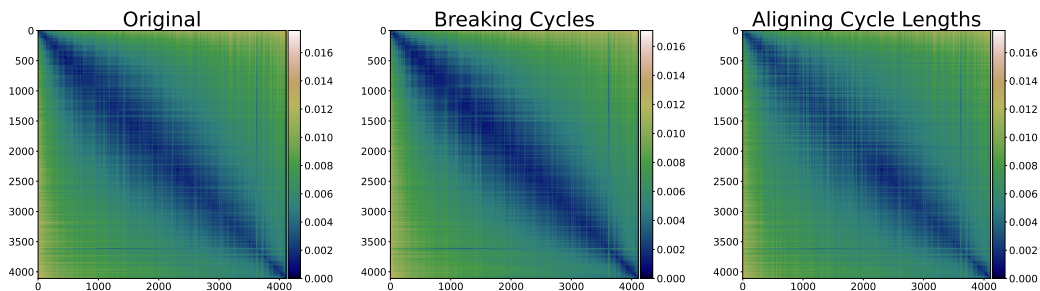


Figure 2. Pairwise graph distance measured by the Wasserstein distance of eigenvalue distributions after breaking cycles and aligning cycle lengths on the NCI109 dataset. Breaking cycles **amplifies the correlation** between eigenvalue distribution and graph size, while aligning cycle lengths **reduces the correlation**.

treat the remaining graphs as graphs of ‘different sizes’. The table shows that the Wasserstein distances of eigenvalue distributions between the graphs of different sizes are significantly larger than the distances between graphs of similar size. Based on the empirical results and Proposition 3.1, the correlation between the eigenvalue distributions and the graph size results in the correlation of the final graph representation and the graph size, which prevents GNNs from generalizing over larger size.

3.3. Key Findings: Size-related Differences in Subgraph Patterns

In this subsection, we aim to identify the subgraph patterns that explain the spectrum differences between small and large graphs. Our empirical analysis pinpointed several peaks in the graph spectrum that match the spectrum of cycles. This motivated us to examine how cycle properties differ in small and large graphs and how these differences are revealed in the spectrum. Specifically, we aim to answer two questions: (Q1) How does the existence of cycles in the graphs influence the spectrum differences? (Q2) How do the variations in cycle lengths contribute to differences in the spectrum? In our analysis, we investigate the properties of the cycles in the cycle basis of each graph.

3.3.1. EXISTENCE OF CYCLES & SPECTRUM: THE IMPACT OF BREAKING CYCLES

To understand how the existence of cycles in the graphs influences the spectrum differences, we break all basis cycles with minimal edge removal while maintaining the same number of disconnected components, according to the details and algorithm given in Appendix E.1. We analyze the impact of breaking cycles by assessing the corresponding changes in the spectrum. By following the convention of Section 3.2, in the center of Figure 2, we plot the pairwise graph distance based on eigenvalue distributions of graphs with different sizes after breaking cycles. The blue band along the diagonal of the plot becomes darker and narrower, suggesting a larger spectrum difference between small and large graphs and a stronger correlation between the spectrum and graph size. To evaluate the effects quantitatively, we further compute the changes in the relative spectrum difference and present the results in Table 2. These results indicate that failing to consider cycle information can lead to more significant differences in the spectrum between graphs of varying sizes, potentially causing GNNs to struggle with generalizing effectively to larger graphs.

Table 2. Average Wasserstein distance of eigenvalue distributions between graphs of similar size and graphs of different sizes after breaking cycles and aligning cycle lengths. Relative difference is computed as in Table 1. We use \uparrow (\downarrow) to denote the increase (decrease) in the relative difference compared to not taking the corresponding action. Breaking cycles results in a larger relative difference, while aligning cycle lengths reduces the relative difference.

Datasets	Breaking cycles			Aligning cycle lengths		
	Different sizes	Similar size	Δ relative difference	Different sizes	Similar size	Δ relative difference
BBBP	0.00545	0.00152	\uparrow 50%	0.00565	0.00211	\downarrow 41%
BACE	0.00420	0.00148	\uparrow 6%	0.00417	0.00176	\downarrow 41%
NCII	0.00547	0.00173	\uparrow 53%	0.00566	0.00242	\downarrow 31%
NCII09	0.00548	0.00174	\uparrow 52%	0.00568	0.00245	\downarrow 31%
PROTEINS	0.00670	0.00212	\uparrow 31%	0.00763	0.00302	\downarrow 41%

3.3.2. CYCLE LENGTH & SPECTRUM: ALIGNING CYCLE LENGTHS

In Section 3.3.1, we showed that cycle information is crucial for GNNs to achieve size generalizability. We now further explore what cycle information helps reduce the spectrum difference between small and large graphs. To facilitate our exploration, we divide each real-world dataset into two subsets: one subset contains small graphs, and the other subset contains graphs of significantly larger size. Further details regarding this dataset split can be found in Appendix B. Using this dataset split, we observe a significant difference in the cycle lengths for small and large graphs (Appendix E.1). As described in Appendix E.1, to reduce that difference, we align the average cycle lengths between small and large graphs by randomly inserting redundant nodes to increase the cycle lengths in small graphs. The rightmost heatmap in Figure 2 shows how the correlation of eigenvalue distributions and graph size changes after aligning cycle lengths. We observe a lighter blue band along the diagonal, which suggests a weaker correlation between the spectrum and graph size. Furthermore, Table 2 quantitatively presents the changes in the relative spectrum difference between small and large graphs. We observe that aligning cycle lengths results in reduced disparities in the spectrum between graphs of different sizes. This indicates that GNNs capable of generalizing across varying cycle lengths may exhibit better size generalizability. In Appendix E.2, we show that our approach of aligning the cycle lengths is more effective at reducing the spectrum disparities than randomly adding the same number of nodes and edges. Importantly, our observation on cycle length variation differs from the assumptions in (Bevilacqua et al., 2021). While they assume the density invariance of the induced k -sized subgraphs, we observe the absence of large cycles in small graphs, indicating a lack of density invariance for cycles.

4. Methodology: Size-insensitive Attention

Our findings in Section 3 suggest that GNNs with better ability to identify cycles and generalize over cycle lengths may have better size generalizability on biological graphs.

However, recent work (Chen et al., 2020) has found that most GNNs are incapable of learning cycle information. Inspired by these, we propose to incorporate cycle information into GNNs by encoding it in the features and leveraging them within the attention mechanism to guide the learning process. Specifically, for each graph \mathcal{G} , we obtain its cycle basis \mathcal{C} . Then, for each node $v_i \in \mathcal{G}$, we calculate the average length of the cycle basis to which it belongs:

$$\ell_i = \begin{cases} \frac{\sum_{j=1}^{|\mathcal{C}|} |c_j| \cdot \mathbb{1}_{\{v_i \in c_j\}}}{\sum_{j=1}^{|\mathcal{C}|} \mathbb{1}_{\{v_i \in c_j\}}} & \text{if } v_i \text{ belongs to some cycles} \\ 0 & \text{otherwise,} \end{cases}$$

where $\mathbb{1}_{\{\text{condition}\}}$ is an indicator function that outputs 1 when the condition is met and 0 otherwise. Then we manually construct a two-dimensional feature vector for each node v_i based on its associated cycle information:

$$\mathbf{c}_i = [\mathbb{1}_{\{v_i \in \text{cycle}\}}, \ell_i].$$

We use the structural feature matrix $\mathbf{C} = [\mathbf{c}_1; \dots; \mathbf{c}_N] \in \mathbb{R}^{N \times 2}$ for attention. Since attention weights often diminish with increasing graph size due to the utilization of `Softmax`, we propose scaling the attention weights by the graph size and employing `Global_max` as the global pooling operation to mitigate the impact of graph size. Mathematically, our final graph representation is given by:

$$\mathbf{k} = \text{Softmax}(\mathbf{C}\mathbf{w}_A^T) \cdot N, \quad \mathbf{x}^{\mathcal{G}} = \text{Global_max}(\text{Diag}(\mathbf{k}) \cdot \mathbf{X}^{(\text{Last})})$$

where \mathbf{w}_A^T is a learnable vector, and `Diag(\cdot)` creates a diagonal matrix using the vector as its elements. We note that when we train on small graphs and test on large graphs, some structural features may not be seen in the training, such as certain cycle lengths in the large graphs. We rely on the attention mechanism to generalize to those cases. Though simple as it seems, `SIA` is found more effective in size generalization than expressive GNNs which are good at identifying cycles Table 3.

5. Experiments

In this section, we conduct extensive experiments to evaluate our proposed strategy *SIA*. We aim to answer the following research questions: **(RQ1) Is cycle information helpful for size generalization?**: Do strategies incorporating cycle information effectively enhance the size generalizability of GNNs? **(RQ2) Comparison with other baselines**: How does *SIA* compare to other baseline strategies?

5.1. Setup

Dataset. We use the same biological datasets as in Section 3.2. More details can be found in Appendix B.

Data Preprocessing and Important Training Details. In order to analyze size generalizability, we have four splits for each dataset: `train`, `validation`, `small_test`, and `large_test`, where `large_test` contains graphs with significantly larger sizes. We generate the splits as follows. First, we sort the samples in the dataset by their size. Next, We take the `train`, `validation`, and `small_test` split from the 50% smallest graphs in the dataset. An intuitive way of getting the `large_test` split is to take the top k largest graphs. However, doing so would result in severe label skewness (class imbalances) between the `small_test` and the `large_test` as demonstrated by Table 5 in Appendix C. To avoid such a severe label shift, we select the same number of graphs per class as in the `small_test` subset, starting from the largest graph within each class. This way guarantees that the label distribution between `small_test` and `large_test` is the same, while ensuring that the graph size in the latter is 2-10 times larger. Nevertheless, the smallest 50% samples still have significant **class imbalance**. To address this issue, we use upsampling during training throughout the experiments, and we use **F1** as the metric to measure the model performance. More details about data preprocessing, hyperparameters, and training can be found in Appendix C and Appendix G.

Baselines. We use six neural network models as our GNN backbones. Each model consists of three layers, with a global max pooling layer employed in the final layer. The baseline models are: Multilayer Perceptron (MLP), GCN (Kipf & Welling, 2017), GAT (Veličković et al., 2018), GIN (Xu et al., 2018), FAGCN (Bo et al., 2021), and GN-NML3 (Balcilar et al., 2021b). We integrate seven model-agnostic strategies with these GNN backbones. We use (1) `+SIA` to denote our proposed size-insensitive attention method. To further validate that cycle information is helpful for size generalization, we propose two additional baselines: (2) `+SSL` introduces a self-supervised loss in addition to the standard classification loss, where the auxiliary task is to predict whether a node is part of a cycle; and (3) `+AugCyc` reduces the discrepancy between small and large graphs by augmenting the training set through the extension of cycle lengths. Further details about `+SSL` and `+AugCyc` can be

found in Appendix D. We also compare with other model-agnostic strategies: (4) `SizeShiftReg` (Buffelli et al., 2022) (`+SSR`), a regularization based on the idea of simulating a shift in the size of the training graphs using coarsening techniques; (5) `RPGNN` (Murphy et al., 2019) (`+RPGNN`), an expressive model for arbitrary-sized graphs; two versions of `CIGA` ((6)`+CIGAv1` & (7)`+CIGAv2`) (Chen et al., 2022), a causal model good at handling out-of-distribution problems on graphs. Besides these model-agnostic strategies, our baselines also include an expressive model (8) `SMP` (Vignac et al., 2020) (`SMP`), which excels at the cycle detection task.

5.2. (RQ1) Is cycle information helpful for size-generalization?

In this section, we aim to evaluate whether cycle information helps enhance the size generalizability of GNNs. We answer this question by evaluating three strategies: `+SIA`, `+SSL`, and `+AugCyc`. The two latter strategies incorporate cycle information through either a self-supervised auxiliary task or direct augmentation and are detailed in Appendix D.

As mentioned in Section 2.2, we evaluate the size generalizability of GNNs by training them on small graphs and testing their graph classification performance on large graphs. Better size generalizability translates into better performance on large graphs. Table 3 showcases the size generalizability results for our three proposed cycle-aware strategies, which we evaluate across five distinct datasets and six different backbone models. Notably, to better compare different strategies, the last column gives the average improvements compared with the original model evaluated across all datasets.

First, all of the cycle-aware strategies consistently lead to improvements in large test datasets without sacrificing the performance on small graphs. On average, these enhancements can reach up to 8.4%, affirming the effectiveness of cycle information in improving GNN size generalizability, as discussed in Section 3. Second, it is worth noting that cycle lengths provide more valuable information for enhancing size generalizability of GNNs. This is evident from the consistently better performance of the strategies `+AugCyc` and `+SIA` compared to the `+SSL` strategy on large test graphs, which solely predicts whether a node belongs to a cycle in the auxiliary task. Third, the simple attention-based strategy `+SIA` achieves the best overall performance improvements in all scenarios. On average, the `+SIA` strategy enhances both in-distribution and out-of-distribution generalization, while `+SSL` and `+AugCyc` excel particularly in out-of-distribution generalization. Additionally, `+SIA` achieves the highest average improvements on large test graphs. We attribute this to the challenges GNNs face in effectively learning cycle information, as shown in recent

Table 3. Size generalizability evaluated by the graph classification performance on small and large test graphs. The performance is reported by the average F1 scores and its standard deviation. The rightmost column denotes the average improvements compared with the original performance using the same backbone model across five different datasets. The largest average improvement within the same model and small/large category is highlighted in orange. All strategies enhance GNNs’ size generalizability, with +SIA surprisingly emerging as the most effective method.

Datasets	BBBP		BACE		PROTEINS		NCII		NCI109		Avg Improv	
	Small	Large	Small	Large	Small	Large	Small	Large	Small	Large	Small	Large
MLP	90.36±0.71	55.61±3.37	61.06±5.79	21.06±7.89	36.15±2.28	21.55±1.34	36.43±3.89	3.36±2.87	35.87±4.23	4.65±3.72	-	-
MLP+SSL	90.90±1.76	62.56±5.48	58.57±8.85	23.01±11.95	35.00±2.8	20.88±1.64	34.71±1.33	2.86±0.78	37.29±4.69	6.34±4.78	-0.68	+1.88
MLP+AugCyc	90.72±2.70	57.86±4.74	59.88±7.33	26.50±14.97	37.29±0.0	22.22±0.0	36.98±2.29	2.64±2.1	40.59±3.86	8.41±3.71	+1.12	+2.28
MLP+SIA	90.38±1.05	62.79±7.55	60.85±7.83	21.79±15.07	40.68±3.56	33.57±11.87	35.42±3.83	3.26±2.55	39.20±2.96	12.2±5.05	+1.33	+5.48
GCN	91.37±0.59	68.59±7.47	63.68±6.63	28.72±14.26	72.35±2.58	40.57±7.67	54.91±2.37	28.80±7.57	60.83±1.92	30.45±4.34	-	-
GCN+SSL	92.66±1.21	73.24±5.71	64.92±4.44	32.84±16.08	72.46±1.58	41.21±6.66	57.43±3.23	32.58±10.08	60.50±3.09	27.35±11.42	+0.97	+2.01
GCN+AugCyc	91.41±1.33	68.08±7.65	63.83±5.44	35.65±7.70	72.87±3.68	54.73±8.24	53.85±3.71	27.39±8.33	62.78±2.98	33.62±3.58	+0.32	+4.47
GCN+SIA	91.32±0.73	71.66±6.99	64.35±9.76	24.24±17.03	73.84±3.65	58.74±9.49	59.78±1.65	45.70±6.70	60.32±2.90	38.78±4.55	+1.29	+8.40
GAT	91.27±1.43	68.35±7.02	69.73±2.05	42.23±11.18	72.25±4.25	43.86±6.82	58.22±2.86	49.36±4.12	64.39±3.29	38.36±8.93	-	-
GAT+SSL	91.65±0.92	74.24±7.34	71.20±2.04	40.88±10.81	74.20±1.46	49.30±5.56	59.47±2.89	51.85±4.03	66.79±3.56	42.20±6.71	+1.49	+3.26
GAT+AugCyc	92.41±1.29	69.57±2.89	68.39±6.06	40.73±13.4	74.99±1.89	59.80±7.27	56.23±3.85	49.37±7.52	64.07±3.46	45.25±9.19	+0.05	+4.51
GAT+SIA	91.88±2.12	74.87±5.62	69.64±6.79	43.87±7.98	75.35±3.28	62.71±4.98	61.42±1.07	55.73±12.98	63.27±3.15	45.97±7.74	+1.14	+8.20
GIN	88.28±2.39	66.67±5.55	57.02±6.48	22.97±10.26	74.55±4.27	50.20±5.36	62.17±3.86	44.26±7.03	62.42±2.77	33.23±6.77	-	-
GIN+SSL	91.13±1.32	68.67±9.75	56.46±8.59	23.91±10.64	75.47±1.15	48.14±4.00	61.18±3.53	46.47±9.86	63.11±4.05	35.0±11.43	+0.58	+0.97
GIN+AugCyc	92.56±1.17	77.69±5.63	58.30±5.29	23.89±13.17	74.56±2.92	51.02±8.42	62.70±0.94	46.76±5.34	64.56±5.45	37.16±5.86	+1.65	+3.84
GIN+SIA	92.70±0.45	75.99±4.74	61.30±6.77	24.42±16.37	74.88±4.24	51.36±7.76	62.83±1.07	42.82±8.92	63.00±4.24	41.65±4.19	+2.05	+3.78
FAGCN	90.58±1.72	64.93±7.62	62.96±2.12	24.65±11.71	70.03±5.20	42.34±6.61	43.51±4.29	10.16±7.80	55.78±3.5	22.65±12.87	-	-
FAGCN+SSL	91.55±2.51	67.56±5.48	64.67±3.88	35.46±16.52	66.97±1.75	48.06±8.33	46.42±6.08	12.11±5.39	56.04±4.29	23.99±10.57	+0.56	+4.49
FAGCN+AugCyc	91.30±2.26	71.44±6.45	57.68±3.38	26.41±23.39	68.85±16.12	44.39±16.89	39.48±4.99	10.98±5.45	55.30±3.46	24.59±9.19	-2.05	+2.62
FAGCN+SIA	90.17±2.83	74.65±9.13	62.40±3.36	30.35±13.48	71.30±5.79	48.94±10.62	46.95±5.71	10.99±7.50	52.82±6.28	19.08±5.32	+0.16	+3.86
GNNML3	92.01±1.56	64.18±6.99	62.31±4.90	32.94±12.86	71.59±3.5	40.74±15.0	63.73±4.67	51.75±9.05	59.39±3.76	33.80±11.19	-	-
GNNML3+SSL	92.96±1.54	64.18±8.62	65.65±5.69	31.78±12.72	74.41±3.21	56.81±3.49	63.91±3.34	48.84±10.07	61.01±2.44	35.13±9.49	+1.78	+2.67
GNNML3+AugCyc	91.38±2.92	69.82±5.51	63.36±2.78	32.59±10.32	70.54±5.00	38.79±5.21	62.30±3.27	55.57±11.73	58.18±3.17	41.30±14.75	-0.65	+2.93
GNNML3+SIA	92.70±0.81	70.43±6.36	64.57±2.72	37.73±7.68	69.32±3.79	48.94±10.62	63.91±5.81	48.85±12.11	61.58±3.98	49.70±17.85	+0.61	+6.45

literature (Chen et al., 2020). Furthermore, in Appendix F, we conduct an ablation study further demonstrating that the attention mechanism, without considering the cycle information, cannot improve the size generalizability of GNNs.

5.3. (RQ2) Comparison with Other Baselines

We now compare our best-performing strategy, +SIA, with other approaches and present their respective graph classification performances in Table 3. We find that +SIA consistently achieves the best performance compared with other baseline methods. While +RPGNN, +SSR, and +CIGA also enhance the size generalizability of GNNs, the improvements are less pronounced than those of +SIA. Additionally, it’s worth noting that +CIGA_{v1} show sensitivity to hyperparameters. While not explicitly designed for size generalizability, the expressive model SMP demonstrates strong performance on the BBBP dataset due to its cycle detection ability, validating our empirical insights. However, though SMP excels in cycle detection, overall, +SIA consistently outperforms SMP.

6. Related Work

Literature on GNNs’ size generalization presents conflicting views. Empirical studies highlight GNNs’ size generalizability in physics simulation (Sanchez-Gonzalez et al., 2020)

and algorithmic reasoning (Xu et al., 2021). Levie et al. (Levie et al., 2021) theoretically showed that spectral GNNs robustly transfer between graphs with varied sizes when discretizing the same underlying space. Meanwhile, some arguments suggest that GNNs may require additional assistance to achieve size generalizability. For instance, Yan et al. (Yan et al., 2020) and Velivckovic et al. (Veličković et al., 2020) found that neural networks effectively generalize to larger graphs than those used in training when attention weights are properly supervised. Conversely, some argue that GNN performance degrades with size shifts between training and test data, leading to the proposal of various models to mitigate this challenge. For instance, Yehudai et al. (Yehudai et al., 2021) argued that this performance degradation can be attributed to the changes in the local degree patterns. Knyazev et al. (Knyazev et al., 2019) found that using attention with proper thresholding can improve the size generalizability of GNNs. Buffelli et al. (Buffelli et al., 2022) simulated a size shift in the training graphs via graph coarsening and proposed a regularization that makes the model robust to the shift. Bevilacqua et al. (Bevilacqua et al., 2021) used a causal model to learn approximately invariant representations that better extrapolate between train and test data. Chen et al. (Chen et al., 2022) utilized structural causal models for robust out-of-distribution generalization in graph data through invariant subgraph identification and label prediction. Chu et al. (Chu et al., 2023) proposed

Table 4. Size generalizability evaluated with other baselines, following the same rule as in Table 3. +STA consistently and significantly outperforms other strategies regarding size generalizability.

Datasets	BBBP		BACE		PROTEINS		NCII		NCII09		Avg Improv	
	Small	Large	Small	Large	Small	Large	Small	Large	Small	Large	Small	Large
MLP	90.36±0.71	55.61±3.37	61.06±5.79	21.06±7.89	36.15±2.28	21.55±1.34	36.43±3.89	3.36±2.87	35.87±4.23	4.65±3.72	-	-
MLP+RPGNN	90.44±1.03	55.10±7.64	57.80±8.53	21.26±8.20	45.60±2.69	20.71±1.41	35.34±4.35	13.45±25.12	38.60±2.37	10.44±18.77	+1.58	+2.95
MLP+SSR	91.07±0.67	57.02±9.04	60.35±5.36	25.42±4.02	37.15±2.48	22.77±4.28	34.42±1.89	1.27±0.63	38.68±4.70	6.96±4.65	+0.36	+1.44
MLP+CIGAv1	88.15±1.05	54.14±6.07	58.18±10.81	24.99±14.41	34.68±4.23	18.23±2.50	33.52±7.85	8.93±7.48	32.79±1.20	3.19±0.01	-2.51	+0.65
MLP+CIGAv2	88.08±3.84	61.70±13.15	57.46±4.71	18.43±16.73	38.28±4.23	24.87±5.62	35.77±7.55	4.22±6.89	38.45±3.68	4.55±1.28	-0.37	+1.51
MLP+StIA	90.38±1.05	62.79±7.55	60.85±7.83	21.79±15.07	40.68±3.56	33.57±11.87	35.42±3.83	3.26±2.55	39.20±2.96	12.2±0.58	+1.33	+5.48
GCN	91.37±0.59	68.59±7.47	63.68±6.63	28.72±14.26	72.35±2.58	40.57±7.67	54.91±2.37	28.80±7.57	60.83±1.92	30.45±4.34	-	-
GCN+RPGNN	92.27±0.81	68.69±6.58	63.70±1.06	33.86±13.91	74.74±3.75	24.61±10.08	58.88±2.03	34.68±10.77	63.10±1.86	39.69±5.88	+1.91	+0.88
GCN+SSR	91.19±1.14	68.15±6.38	66.01±2.51	31.64±9.96	73.51±2.91	43.33±5.19	59.60±2.62	35.01±7.13	59.78±2.71	33.11±6.44	+1.39	+2.82
GCN+CIGAv1	90.55±1.32	66.55±5.80	66.66±5.72	28.51±8.64	72.64±1.81	54.67±6.08	58.52±4.88	40.82±11.14	59.09±3.50	25.82±7.81	+0.86	+3.85
GCN+CIGAv2	89.45±3.60	69.71±8.20	65.02±1.80	35.42±12.36	72.15±3.86	60.12±6.84	57.89±3.74	35.42±10.75	58.12±5.97	28.51±10.10	-0.10	+6.41
GCN+StIA	91.32±0.73	71.66±6.99	64.35±9.76	24.24±17.03	73.84±3.65	58.74±9.49	59.78±1.65	45.70±6.70	60.32±2.30	38.78±4.55	+1.29	+8.40
GAT	91.27±1.43	68.35±7.02	69.73±2.05	42.23±11.18	72.25±4.25	43.86±6.82	58.22±2.86	49.36±4.12	64.39±3.29	38.36±8.93	-	-
GAT+RPGNN	91.76±1.69	65.85±5.37	69.97±2.17	39.27±13.50	72.89±3.35	38.49±6.14	59.31±5.51	58.18±5.76	65.52±1.94	44.15±5.76	-0.75	+0.76
GAT+SSR	91.98±0.66	74.83±4.35	66.03±3.83	41.41±11.8	74.72±3.51	44.81±8.59	60.68±1.95	49.64±5.26	66.73±1.65	41.14±4.41	+0.86	+1.93
GAT+CIGAv1	89.53±1.51	67.35±8.74	67.18±5.12	39.88±18.64	73.28±4.87	48.56±5.42	59.52±3.27	54.35±11.85	66.82±2.03	50.62±4.85	+0.09	+3.72
GAT+CIGAv2	90.92±1.43	72.08±7.09	66.57±4.91	40.93±19.35	74.68±7.54	60.88±3.48	56.88±24.40	54.28±22.63	66.78±3.20	52.62±7.98	-0.01	+7.73
GAT+StIA	91.88±2.12	74.87±5.62	69.64±6.79	43.87±9.98	75.35±3.28	62.71±4.98	61.42±1.07	55.73±12.98	63.27±3.15	45.97±7.74	+1.14	+8.20
GIN	88.28±2.39	66.67±5.55	57.02±6.48	22.97±10.26	74.55±4.27	50.20±5.36	62.17±3.86	44.26±7.03	62.42±2.77	33.23±6.77	-	-
GIN+RPGNN	89.59±1.33	69.23±8.05	57.23±7.07	16.28±9.31	71.63±5.85	45.11±15.98	61.59±4.12	48.86±5.88	62.27±2.33	44.04±7.06	-0.43	+1.24
GIN+SSR	89.00±1.77	68.84±6.01	59.83±2.34	21.28±19.26	72.46±2.86	55.46±15.95	62.54±1.30	48.73±8.62	61.05±3.37	35.63±7.29	+0.09	+2.52
GIN+CIGAv1	91.01±1.59	74.85±10.41	60.58±7.15	23.78±17.58	75.32±16.25	54.83±9.87	61.94±1.08	45.85±5.83	61.55±12.55	35.88±7.77	+1.19	+3.57
GIN+CIGAv2	90.66±1.72	75.80±14.30	63.02±1.80	22.42±12.36	73.25±5.42	53.35±8.76	64.42±5.35	45.37±5.12	59.52±4.68	38.42±5.68	+1.29	+3.61
GIN+StIA	92.70±0.45	75.99±4.74	61.30±6.77	24.42±16.37	74.88±4.24	51.36±7.76	62.83±1.07	42.82±8.92	63.00±4.24	41.65±4.19	+2.05	+3.78
FAGCN	90.58±1.72	64.93±7.62	62.96±2.12	24.65±11.71	70.03±5.20	42.34±6.61	43.51±4.29	10.16±7.80	55.78±3.5	22.65±12.87	-	-
FAGCN+RPGNN	90.43±2.58	69.58±11.71	61.00±5.91	20.94±12.62	68.71±3.58	43.58±12.21	44.55±5.82	12.22±5.95	57.03±1.08	21.86±13.32	-0.23	+0.69
FAGCN+SSR	88.95±2.16	70.12±9.49	64.12±2.57	22.37±7.80	67.92±3.00	42.27±8.69	47.47±2.77	14.69±8.22	55.66±3.37	22.35±9.35	+0.25	+1.41
FAGCN+CIGAv1	91.08±1.48	69.29±3.35	62.66±5.72	28.51±8.64	68.58±6.19	57.79±10.45	40.93±10.69	9.45±11.16	48.07±5.70	15.11±5.82	+1.19	+3.57
FAGCN+CIGAv2	92.08±1.70	68.37±9.67	60.37±4.65	22.29±15.00	69.45±4.97	60.28±12.24	44.27±6.74	15.88±10.25	50.25±4.44	16.22±7.74	-1.29	+3.66
FAGCN+StIA	90.17±2.83	74.65±9.13	62.40±3.36	30.35±13.48	71.30±5.79	48.94±10.62	46.95±5.71	10.99±7.50	52.82±6.28	19.08±5.32	+0.16	+3.86
GNNML3	92.01±1.56	64.18±6.99	62.31±4.90	32.94±12.86	71.59±3.5	40.74±15.0	63.73±4.67	51.75±9.05	59.39±3.76	33.80±11.19	-	-
GNNML3+RPGNN	92.57±1.45	72.30±9.54	61.85±3.67	27.54±12.03	70.48±2.46	38.61±14.61	64.60±2.14	50.25±8.65	60.22±2.40	36.88±15.93	+0.14	+0.43
GNNML3+SSR	91.86±1.30	69.96±5.50	64.95±2.82	26.56±4.68	74.33±1.85	49.02±7.42	63.19±4.35	54.30±10.33	63.27±2.74	45.74±11.47	+1.41	+4.43
GNNML3+CIGAv1	91.25±4.67	72.80±5.88	64.23±2.10	34.95±15.92	73.89±4.73	52.01±12.59	61.89±4.53	45.25±7.80	60.95±3.44	38.80±12.36	+0.64	+4.08
GNNML3+CIGAv2	89.61±1.46	67.17±5.94	64.19±5.36	27.28±12.79	75.07±2.64	54.50±9.29	60.28±4.56	46.25±10.42	60.60±1.16	42.19±12.61	+0.14	+2.80
GNNML3+StIA	92.70±0.81	70.43±6.36	64.57±2.72	37.73±7.68	69.32±3.79	48.94±10.62	63.91±5.81	48.85±12.11	61.58±3.98	49.70±17.85	+0.61	+6.45
SMP	92.30±2.62	80.25±5.98	61.32±5.69	28.71±6.55	76.87±1.90	45.69±15.96	51.09±6.39	22.98±16.26	49.15±6.92	30.73±11.30	-	-

a Wasserstein barycenter matching (WBM) layer to address the slow uncontrollable convergence rate w.r.t. graph size. Zhou et al. (Zhou et al., 2022) studied the size OOD problem in the task of link prediction. Ji et al. (Ji et al., 2022) curated OOD datasets for AI-aided drug discovery. Our study stands out as the first to utilize spectral analysis to characterize the types of size-induced distribution shifts, shedding light on the underlying causes that hinder GNNs from effectively generalizing to large graphs. Some expressive models also exhibit robustness in size generalization. Murphy et al. (Murphy et al., 2019) proposed an expressive model-agnostic framework that learns graph representations invariant to graph isomorphism given variable-length inputs. Clement et al. (Vignac et al., 2020) proposed an expressive graph neural network that performs well on difficult structural tasks, such as cycle detection and diameter computation. Our study validates that expressive models excelling in cycle-related tasks demonstrate good size generalizability.

7. Conclusion

In conclusion, our work extensively characterizes size-induced distribution shifts and evaluates their impact on GNNs’ generalizability to significantly larger test graphs compared to the training set. Spectral analysis on real-world biological data reveals a strong correlation between graph spectrum and size, which hinders GNNs’ size generalization. We identify the pivotal role of cycle-related information in reducing spectral differences between small and large graphs. Motivated by these findings, we introduce a size-insensitive attention strategy that can be integrated with any GNN architectures. Our empirical findings suggest that cycle information is crucial for size generalization and our proposed method significantly enhances the size generalizability of GNNs. This research provides valuable insights for enhancing GNN generalization across varying graph sizes.

Impact Statements

This paper presents work whose goal is to advance the field of machine learning. Our research reveals important insights in the scientific domain, i.e., biology, contributing to the enhancement and progress of the field.

References

- Balcilar, M., Guillaume, R., Héroux, P., Gaüzère, B., Adam, S., and Honeine, P. Analyzing the expressive power of graph neural networks in a spectral perspective. In *Proceedings of the International Conference on Learning Representations (ICLR)*, 2021a.
- Balcilar, M., Héroux, P., Gauzere, B., Vasseur, P., Adam, S., and Honeine, P. Breaking the limits of message passing graph neural networks. In *International Conference on Machine Learning*, pp. 599–608. PMLR, 2021b.
- Berlingerio, M., Koutra, D., Eliassi-Rad, T., and Faloutsos, C. A scalable approach to size-independent network similarity. *ArXiv Preprint ArXiv: 12092684*, 2012.
- Bevilacqua, B., Zhou, Y., and Ribeiro, B. Size-invariant graph representations for graph classification extrapolations. In *International Conference on Machine Learning*, pp. 837–851. PMLR, 2021.
- Bo, D., Wang, X., Shi, C., and Shen, H. Beyond low-frequency information in graph convolutional networks. *arXiv preprint arXiv:2101.00797*, 2021.
- Buffelli, D., Lio, P., and Vandin, F. Sizeshiftreg: a regularization method for improving size-generalization in graph neural networks. In *Advances in Neural Information Processing Systems*, 2022.
- Chen, Y., Zhang, Y., Bian, Y., Yang, H., Kaili, M., Xie, B., Liu, T., Han, B., and Cheng, J. Learning causally invariant representations for out-of-distribution generalization on graphs. *Advances in Neural Information Processing Systems*, 35:22131–22148, 2022.
- Chen, Z., Chen, L., Villar, S., and Bruna, J. Can graph neural networks count substructures? *Advances in neural information processing systems*, 33:10383–10395, 2020.
- Chu, X., Jin, Y., Wang, X., Zhang, S., Wang, Y., Zhu, W., and Mei, H. Wasserstein barycenter matching for graph size generalization of message passing neural networks. In *International Conference on Machine Learning*, pp. 6158–6184. PMLR, 2023.
- Defferrard, M., Bresson, X., and Vandergheynst, P. Convolutional neural networks on graphs with fast localized spectral filtering. In *NeurIPS*, 2016.
- Gilmer, J., Schoenholz, S. S., Riley, P. F., Vinyals, O., and Dahl, G. E. Neural message passing for quantum chemistry. In *International conference on machine learning*, pp. 1263–1272. PMLR, 2017.
- Hamilton, W., Ying, Z., and Leskovec, J. Inductive representation learning on large graphs. In *NeurIPS*, 2017.
- Hu, W., Fey, M., Zitnik, M., Dong, Y., Ren, H., Liu, B., Catasta, M., and Leskovec, J. Open graph benchmark: Datasets for machine learning on graphs. *arXiv preprint arXiv:2005.00687*, 2020a.
- Hu, W., Fey, M., Zitnik, M., Dong, Y., Ren, H., Liu, B., Catasta, M., and Leskovec, J. Open graph benchmark: Datasets for machine learning on graphs. *Advances in neural information processing systems*, 33:22118–22133, 2020b.
- Hu, W., Liu, B., Gomes, J., Zitnik, M., Liang, P., Pande, V., and Leskovec, J. Strategies for pre-training graph neural networks. In *International Conference on Learning Representations (ICLR)*, 2020c.
- Ji, Y., Zhang, L., Wu, J., Wu, B., Huang, L.-K., Xu, T., Rong, Y., Li, L., Ren, J., Xue, D., et al. Drugood: Out-of-distribution (ood) dataset curator and benchmark for ai-aided drug discovery—a focus on affinity prediction problems with noise annotations. *arXiv preprint arXiv:2201.09637*, 2022.
- Kipf, T. N. and Welling, M. Semi-supervised classification with graph convolutional networks. In *International Conference on Learning Representations (ICLR)*, 2017.
- Knyazev, B., Taylor, G. W., and Amer, M. Understanding attention and generalization in graph neural networks. *Advances in neural information processing systems*, 32, 2019.
- Lee, J. B., Rossi, R., and Kong, X. Graph classification using structural attention. In *Proceedings of the 24th ACM SIGKDD International Conference on Knowledge Discovery & Data Mining*, pp. 1666–1674, 2018.
- Levie, R., Monti, F., Bresson, X., and Bronstein, M. M. Cayleynets: Graph convolutional neural networks with complex rational spectral filters. *IEEE Transactions on Signal Processing*, 67(1):97–109, 2018.
- Levie, R., Huang, W., Bucci, L., Bronstein, M., and Kutyiniok, G. Transferability of spectral graph convolutional neural networks. *The Journal of Machine Learning Research*, 22(1):12462–12520, 2021.
- Morris, C., Kriege, N. M., Bause, F., Kersting, K., Mutzel, P., and Neumann, M. Tudataset: A collection of benchmark datasets for learning with graphs. In *ICML 2020*

- Workshop on Graph Representation Learning and Beyond (GRL+ 2020)*, 2020. URL www.graphlearning.io.
- Murphy, R., Srinivasan, B., Rao, V., and Ribeiro, B. Relational pooling for graph representations. In *International Conference on Machine Learning*, pp. 4663–4673. PMLR, 2019.
- Paton, K. An algorithm for finding a fundamental set of cycles of a graph. *Communications of the ACM*, 12(9): 514–518, 1969.
- Sanchez-Gonzalez, A., Godwin, J., Pfaff, T., Ying, R., Leskovec, J., and Battaglia, P. Learning to simulate complex physics with graph networks. In *International conference on machine learning*, pp. 8459–8468. PMLR, 2020.
- Sysło, M. M. On cycle bases of a graph. *Networks*, 9(2): 123–132, 1979.
- Veličković, P., Cucurull, G., Casanova, A., Romero, A., Liò, P., and Bengio, Y. Graph Attention Networks. *International Conference on Learning Representations (ICLR)*, 2018. URL <https://openreview.net/forum?id=rJXMpikCZ>.
- Veličković, P., Ying, R., Padovano, M., Hadsell, R., and Blundell, C. Neural execution of graph algorithms. In *International Conference on Learning Representations*, 2020.
- Vignac, C., Loukas, A., and Frossard, P. Building powerful and equivariant graph neural networks with structural message-passing. *Advances in neural information processing systems*, 33:14143–14155, 2020.
- Villani, C. et al. *Optimal transport: old and new*, volume 338. Springer, 2009.
- Wale, N. and Karypis, G. Comparison of descriptor spaces for chemical compound retrieval and classification. In *Sixth International Conference on Data Mining (ICDM'06)*, pp. 678–689, 2006. doi: 10.1109/ICDM.2006.39.
- Wu, Z., Ramsundar, B., Feinberg, E. N., Gomes, J., Geniesse, C., Pappu, A. S., Leswing, K., and Pande, V. Moleculenet: a benchmark for molecular machine learning. *Chemical science*, 9(2):513–530, 2018.
- Xu, K., Hu, W., Leskovec, J., and Jegelka, S. How powerful are graph neural networks? *International Conference on Learning Representations*, 2018.
- Xu, K., Zhang, M., Li, J., Du, S. S., Kawarabayashi, K.-i., and Jegelka, S. How neural networks extrapolate: from feedforward to graph neural networks. In *International Conference on Learning Representations (ICLR)*, 2021.
- Yan, Y., Zhu, J., Duda, M., Solarz, E., Sripada, C., and Koutra, D. Groupinn: Grouping-based interpretable neural network for classification of limited, noisy brain data. In *proceedings of the 25th ACM SIGKDD international conference on knowledge discovery & data mining*, pp. 772–782, 2019.
- Yan, Y., Swersky, K., Koutra, D., Ranganathan, P., and Hashemi, M. Neural execution engines: Learning to execute subroutines. *Advances in Neural Information Processing Systems*, 33:17298–17308, 2020.
- Yehudai, G., Fetaya, E., Meirom, E., Chechik, G., and Maron, H. From local structures to size generalization in graph neural networks. In *International Conference on Machine Learning*, pp. 11975–11986. PMLR, 2021.
- Ying, Z., You, J., Morris, C., Ren, X., Hamilton, W., and Leskovec, J. Hierarchical graph representation learning with differentiable pooling. In *NeurIPS*, pp. 4800–4810, 2018.
- Zhang, M., Cui, Z., Neumann, M., and Chen, Y. An end-to-end deep learning architecture for graph classification. In *Proceedings of the AAAI conference on artificial intelligence*, volume 32, 2018.
- Zhou, Y., Kutyniok, G., and Ribeiro, B. Ood link prediction generalization capabilities of message-passing gnns in larger test graphs. *Advances in Neural Information Processing Systems*, 35:20257–20272, 2022.

A. Proposition

In this Appendix, we provide theoretical reasoning for the proposition in Section 3.1.

Without loss of generality, the output of a spectral GNN at the $(l+1)$ -th layer is given by: $\mathbf{X}^{(l+1)} = \sigma(\mathbf{U}f(\mathbf{\Lambda})\mathbf{U}^T\mathbf{X}^{(l)}\mathbf{W}^{(l)})$ (Section 2). To ease our analysis, we rewrite \mathbf{U} , $\mathbf{\Lambda}$ and $\mathbf{X}^{(l)}$ as: $\mathbf{U} = [\mathbf{U}_1, \mathbf{U}_2, \dots, \mathbf{U}_N]$, $\mathbf{\Lambda} = \text{Diag}([\lambda_1, \lambda_2, \dots, \lambda_N])$, and $\mathbf{X}^{(l)} = [\mathbf{X}_1^{(l)}, \mathbf{X}_2^{(l)}, \dots, \mathbf{X}_D^{(l)}]$, respectively. \mathbf{U}_i is the i -th column vector of \mathbf{U} , λ_i is the i -th largest eigenvalue, $\text{Diag}(\cdot)$ creates a matrix with the vector as its diagonal elements, $\mathbf{X}_i^{(l)}$ is the i -th column vector of $\mathbf{X}^{(l)}$, and D is the feature dimension at the l -th layer.

$$\begin{aligned} \mathbf{X}^{(l+1)} &= \sigma([\mathbf{U}_1, \mathbf{U}_2, \dots, \mathbf{U}_N] \cdot \text{Diag}([f(\lambda_1), f(\lambda_2), \dots, f(\lambda_N)]) \cdot ([\mathbf{U}_1, \mathbf{U}_2, \dots, \mathbf{U}_N])^T \\ &\quad \cdot [\mathbf{X}_1^{(l)}, \mathbf{X}_2^{(l)}, \dots, \mathbf{X}_D^{(l)}] \cdot \mathbf{W}^{(l)}) \\ &= \sigma([f(\lambda_1)\mathbf{U}_1, f(\lambda_2)\mathbf{U}_2, \dots, f(\lambda_N)\mathbf{U}_N] \cdot ([\mathbf{U}_1, \mathbf{U}_2, \dots, \mathbf{U}_N])^T \\ &\quad \cdot [\mathbf{X}_1^{(l)}, \mathbf{X}_2^{(l)}, \dots, \mathbf{X}_D^{(l)}] \cdot \mathbf{W}^{(l)}). \end{aligned} \quad (1)$$

Since $\{\mathbf{U}_i : i = 1, \dots, N\}$ are the orthonormal basis of \mathbb{R}^N , $\mathbf{X}_i^{(l)}$ can be expressed as a linear combination of $\{\mathbf{U}_i\}$. Thus, suppose $\mathbf{X}_i^{(l)} = \sum_{j=1,2,\dots,N} \alpha_j^i \mathbf{U}_j$, then Equation 1 can be rewritten as:

$$\begin{aligned} \mathbf{X}^{(l+1)} &= \sigma([f(\lambda_1)\mathbf{U}_1, f(\lambda_2)\mathbf{U}_2, \dots, f(\lambda_N)\mathbf{U}_N] \cdot ([\mathbf{U}_1, \mathbf{U}_2, \dots, \mathbf{U}_N])^T \\ &\quad \cdot [\sum_{j=1,2,\dots,N} \alpha_j^1 \mathbf{U}_j, \dots, \sum_{j=1,2,\dots,N} \alpha_j^D \mathbf{U}_j] \cdot \mathbf{W}^{(l)}) \\ &= \sigma \left([f(\lambda_1)\mathbf{U}_1, f(\lambda_2)\mathbf{U}_2, \dots, f(\lambda_N)\mathbf{U}_N] \cdot \begin{bmatrix} \alpha_1^1 & \alpha_1^2 & \dots & \alpha_1^D \\ \alpha_2^1 & \alpha_2^2 & \dots & \alpha_2^D \\ \dots & \dots & \dots & \dots \\ \alpha_N^1 & \alpha_N^2 & \dots & \alpha_N^D \end{bmatrix} \cdot \mathbf{W}^{(l)} \right) \\ &= \sigma([\sum_{j=1,\dots,N} f(\lambda_j)\alpha_j^1 \mathbf{U}_j, \sum_{j=1,\dots,N} f(\lambda_j)\alpha_j^2 \mathbf{U}_j, \dots, \sum_{j=1,\dots,N} f(\lambda_j)\alpha_j^D \mathbf{U}_j] \cdot \mathbf{W}^{(l)}). \end{aligned} \quad (2)$$

We know that $\alpha_j^i = \mathbf{U}_j^T \cdot \mathbf{X}_i^{(l)} = \text{COSINE}(\mathbf{U}_j, \mathbf{X}_i^{(l)}) \cdot \|\mathbf{X}_i^{(l)}\|_2 = \text{COSINE}(\mathbf{U}_j, \mathbf{X}_i^{(l)}) \cdot \frac{\|\mathbf{X}_i^{(l)}\|_2}{\sqrt{N}} \cdot \sqrt{N}$. Then Equation 2 can be rewritten as:

$$\begin{aligned} \mathbf{X}^{(l+1)} &= \sigma([\sum_{j=1,\dots,N} f(\lambda_j)\text{COSINE}(\mathbf{U}_j, \mathbf{X}_1^{(l)}) \cdot \frac{\|\mathbf{X}_1^{(l)}\|_2}{\sqrt{N}} \cdot (\sqrt{N} \cdot \mathbf{U}_j), \\ &\quad \dots, \sum_{j=1,\dots,N} f(\lambda_j)\text{COSINE}(\mathbf{U}_j, \mathbf{X}_D^{(l)}) \cdot \frac{\|\mathbf{X}_D^{(l)}\|_2}{\sqrt{N}} \cdot (\sqrt{N} \cdot \mathbf{U}_j)] \cdot \mathbf{W}^{(l)}). \end{aligned} \quad (3)$$

The final graph representation is obtained through a global pooling (Section 2), where a set function is applied to each feature dimension. To ensure that the graph representation is irrelevant to the graph size, it is crucial for each column of $\mathbf{X}^{(l+1)}$ to be unaffected by the size. If the distributions of eigenvalues (λ_j), scaled eigenvectors ($\sqrt{N} \cdot \mathbf{U}_j$), and the scalar $\frac{\|\mathbf{X}_i^{(l)}\|_2}{\sqrt{N}}$, are uncorrelated with the graph size, then the graph representation will be size-invariant. It is worth noting that $\mathbf{X}_i^{(l)}$ contains N elements and its 2-norm scales with \sqrt{N} ; and $\|\mathbf{U}_j\|_2 = 1$ and its elements diminish with \sqrt{N} . Hence, we account for the scaling factor \sqrt{N} in both terms. However, the distributions of eigenvalues (Section 3.2) and scaled eigenvectors in real biological graphs are influenced by the graph size. This poses a challenge for the size generalization of GNNs. Importantly, the difference in eigenvalue distributions cannot be attributed to the value range (Berlingerio et al., 2012), as the eigenvalues of a normalized Laplacian matrix and adjacency matrix are constrained within the intervals $[0,2]$ and $[-1,1]$ respectively.

B. Datasets

In this section, we provide additional details about the datasets utilized in our study. We utilize five pre-processed biological datasets, namely BBBP and BACE from the Open Graph Benchmark (Hu et al., 2020b), and PROTEINS, NCI1, and

NCI109 from TuDataset (Morris et al., 2020), for graph classification in our experiments. Each graph in BBBP and BACE represents a molecule, where nodes are atoms, and edges are chemical bonds. Each node has a 9-dimensional feature vector, which contains its atomic number and chirality, as well as other additional atom features such as formal charge and whether the atom is in the ring or not (Hu et al., 2020b). In the PROTEINS dataset, nodes correspond to amino acids, and an edge connects two nodes if their distance is less than 6 Angstroms. Each node is associated with a 3-dimensional feature vector representing the type of secondary structure elements, such as helix, sheet, or turn. Each graph in NCI1 and NCI109 represents a chemical compound: each node stands for an atom and has a one-hot encoded feature representing the corresponding atom type; each edge represents the chemical bonds between the atoms. The description of each dataset is summarized as follows:

- **BBBP**: The blood-brain barrier penetration (BBBP) dataset comes from a study on the modeling and the prediction of barrier permeability. It includes binary labels of over 2000 compounds on their permeability properties (Wu et al., 2018).
- **BACE**: The BACE dataset provides quantitative (IC50) and qualitative (binary label) binding results for a set of inhibitors of human β -secretase 1 (BACE-1). It contains 1522 compounds with their 2D structures and binary labels (Wu et al., 2018).
- **PROTEINS**: The PROTEINS dataset comprises the macromolecule graphs of proteins and binary labels of the protein function (being an enzyme or not) for a total of 1113 samples (Morris et al., 2020).
- **NCI1 & NCI109**: The NCI1 and NCI109 are two balanced subsets of chemical compounds screened for their activity against non-small cell lung cancer and ovarian cancer cell lines, respectively (Wale & Karypis, 2006). NCI1 contains a total of 4110 samples and NCI109 contains a total of 4117 samples.

C. Data Splits and Pre-processing

Table 5. Label distributions of BBBP, BACE, PROTEINS, NCI1 and NCI109 in the entire dataset, the smallest 50% subset, and the largest 10% subset.

Dataset		BBBP	BACE	PROTEINS	NCI1	NCI109
Entire Dataset	Number of Class 0 Samples	479	822	663	2053	2048
	Number of Class 1 Samples	1560	691	450	2057	2079
Smallest 50%	Number of Class 0 Samples	138	501	232	1283	1283
	Number of Class 1 Samples	882	256	325	772	781
Largest 10%	Number of Class 0 Samples	122	53	101	78	87
	Number of Class 1 Samples	82	99	11	333	326

In this section, we discuss the techniques employed to address the challenges of class imbalance and label distribution shifts between small and large graphs. Given our emphasis on size shift, we preprocess the dataset to mitigate the influence from other distribution shifts.

For each dataset, Table 5 presents the respective class size in the whole dataset, the smallest 50% subset, and the largest 10% subset. This table reveals two main issues. Firstly, many datasets (BBBP, BACE, and PROTEINS) demonstrate imbalanced label distributions. Secondly, both the smallest 50% and the largest 10% graphs exhibit class imbalance, and there is a notable difference in the label distribution between these subsets. To mitigate these issues, we carefully split our data and apply the upsampling technique.

Data splits. For each dataset, we create four distinct splits: train, validation, small_test, and large_test. The large_test split consists of graphs with significantly larger sizes compared to the other splits. To generate the train, validation, and small_test subsets, we initially select the smallest 50% of graphs from the dataset. The division among these subsets follows a ratio of 0.7:0.15:0.15, respectively. Importantly, we ensure that the data is split for each class using the same ratio, thereby

maintaining consistent label distributions across the train, validation, and small_test subsets. Next, we generate the large_test subset by selecting the same number of graphs per class as in the small_test subset. The selection process begins with the largest graph within each class and ensures that the large_test subset maintains the same class distribution as the small_test subset. Table 6 shows the class size obtained after applying this operation.

Upsampling. As can be seen in Table 5, even after performing the appropriate data split, each dataset still exhibits varying degrees of class imbalance. To avoid training an extremely biased model, we adopt the upsampling technique during the training process. Specifically, we upsample the graphs in class 0 of BBBP at a ratio of 6, the graphs in class 1 of BACE at a ratio of 2, $\frac{2}{3}$ of the graphs in class 0 of PROTEINS at a ratio of 2, and $\frac{2}{3}$ of the graphs in class 1 of NCI1 and NCI109 at a ratio of 2.

Table 6. Label distributions after proper data splits. both the Both the small_test and large_test subsets now have the same class distribution.

Dataset		BBBP	BACE	PROTEINS	NCI1	NCI109
Train	Number of Class 0 Samples	96	350	140	898	898
	Number of Class 1 Samples	617	179	210	540	546
Val	Number of Class 0 Samples	22	76	30	193	193
	Number of Class 1 Samples	133	39	46	117	118
Small_test	Number of Class 0 Samples	20	75	30	192	192
	Number of Class 1 Samples	132	38	45	115	117
Large_test	Number of Class 0 Samples	20	75	30	192	192
	Number of Class 1 Samples	132	38	45	115	117

D. Additional Cycle-aware Baselines

In this section, we introduce the two additional baselines that are used to evaluate the effectiveness of cycle information in enhancing size generalization: +SSL and +AugCyc, which we briefly introduce in Section 5.

D.1. Self-supervised Auxiliary Task (+SSL)

This approach utilizes a self-supervised auxiliary task to enhance the node representations with cycle-related information. The auxiliary task is to predict whether a node belongs to a cycle. We do not utilize cycle lengths as labels because large test graphs may have cycle lengths not present in the training data. Formally, let $X^{(Last)}$ denote the node representations obtained after the last graph convolution. The conventional way of learning is to directly apply a pooling operator and then minimize the loss function for label supervision as below:

$$\mathcal{L}_{label} = \text{CrossEntropy}(\text{Linear}(\text{Pooling}(\mathbf{X}^{(Last)}), y^{\mathcal{G}}))$$

where $y^{\mathcal{G}}$ is the ground truth label for the graph. In this approach, we incorporate an additional loss that aims to diffuse cycle-related information into the node representations through supervision:

$$\mathcal{L}_{cycle} = \text{CrossEntropy}(\text{MLP}(\mathbf{X}^{(Last)}), \mathbf{y}_{cycle})$$

where \mathbf{y}_{cycle} is an indicator vector denoting whether a node belongs to a cycle. To sum up, the total loss is given by:

$$\mathcal{L} = \mathcal{L}_{label} + \lambda \mathcal{L}_{cycle}$$

where λ is a hyperparameter tuned via cross-validation.

D.2. Augmentation (+AugCyc)

This approach aims to reduce the discrepancy between small and large graphs through direct augmentation for the small training graphs. We augment the training graphs by extending the cycle lengths such that the average cycle length and standard deviation align with those in large graphs. To achieve this augmentation, we use the algorithm detailed in Appendix E.1. Additionally, we replicate the features from the nodes with the lowest degrees in the same cycle to populate the features for the newly added nodes. Last, we feed the augmented training graphs to GNNs for graph classification.

E. Details and Discussions on Breaking Cycles and Aligning Cycle Lengths

In this section, we begin by elaborating on the procedures for breaking cycles and aligning cycle lengths, which we briefly introduced in Section 3. Then, we present the results of an ablation study on adding nodes randomly (instead of based on the underlying cycles).

E.1. Implementation Details

Our **cycle-breaking algorithm** is designed to remove all cycles in the graph with minimal edge removal while maintaining the current number of disconnected components. This approach minimally perturbs the graph while focusing on cycles. To achieve this, we begin by obtaining the cycle basis \mathcal{C} (Section 2) of the input graph \mathcal{G} . Breaking all cycles can be accomplished by removing just one edge from each cycle in the basis. To ensure that this edge removal process does not increase the number of disconnected components, we propose a backtracking algorithm (Algorithm 1). We note that while it is possible for Algorithm 1 to have failure cases, luckily, in all the datasets we have examined, we have not observed any instances where cycle breaking fails (i.e., Algorithm 1 returning False).

Algorithm 1 Cycle Breaking

```

1: procedure CYCLEBACKTRACKING( $i$ : index integer,  $\mathcal{G}$ : input graph,  $\mathcal{C}$ : a list of cycle basis)
2:   if  $i == \text{len}(\mathcal{C})$  then
3:     return True
4:    $N_{\text{before}} \leftarrow \text{NumberOfConnectedComponent}(\mathcal{G})$ 
5:   for edge pair  $\varepsilon$  in  $\mathcal{C}_i$  do
6:      $\mathcal{G} \leftarrow \text{Remove}(\varepsilon)$ 
7:      $N_{\text{after}} \leftarrow \text{NumberOfConnectedComponent}(\mathcal{G})$ 
8:     if  $N_{\text{before}} == N_{\text{after}}$  then
9:       if CycleBacktracking( $i + 1, \mathcal{G}, \mathcal{C}$ ) then
10:        return True
11:      $\mathcal{G} \leftarrow \text{add}(\varepsilon)$ 
12:   return False

```

Before delving into the cycle length alignment algorithm, we first present the average statistics for both the small and large graphs, as outlined in Table 7. To derive these statistics, we obtain the cycle basis (Section 2) for each input graph and compute the average length across the cycles in that basis. Then, we calculate the average cycle length by further averaging it over all the graphs within the small and large datasets, respectively. Note that small and large graphs differ in both the mean and the standard deviation of cycle lengths, indicating that large graphs may contain notably long cycles that are not present in the small graphs.

Table 7. Average cycle lengths for small and large graphs before and after cycle length alignment. Small and large graphs in real biological datasets originally differ in cycle length and such difference is reduced after cycle length alignment.

	BBBP		BACE		NCII		NCII09		PROTEINS	
	small	large								
before alignment	5.56 ± 1.39	6.54 ± 3.52	5.70 ± 0.56	6.50 ± 2.01	5.64 ± 1.19	7.04 ± 3.05	5.59 ± 1.25	7.06 ± 2.88	3.20 ± 0.34	6.24 ± 2.75
after alignment	6.50 ± 3.12	6.54 ± 3.52	6.48 ± 2.08	6.50 ± 2.01	6.97 ± 2.97	7.04 ± 3.05	6.86 ± 3.02	7.06 ± 2.88	5.97 ± 3.03	6.24 ± 2.75

Our **cycle length alignment algorithm** aligns both the *mean* and *std* of average cycle lengths between small and large graphs. This is achieved by selectively increasing the cycle length of a subset of small graphs. Formally, we present our algorithm in Algorithm 3. It has two hyperparameters: n , which controls the maximum cycle length increments one graph can get, and \mathcal{R} , which controls the portion of small graphs whose cycle lengths will be increased. We tune these hyperparameters in order to best align the cycle length of small graphs with that of large graphs. We tune n over $[2, 3, 4, 5, 6, 7]$ and \mathcal{R} over $[1, 2, 3, 4, 5, 6, 7, 8]$, and identify $n = 7, \mathcal{R} = 8$ for BBBP, $n = 6, \mathcal{R} = 8$ for BACE, $n = 6, \mathcal{R} = 5$ for NCI1, $n = 6, \mathcal{R} = 5$ for NCI109 and $n = 5, \mathcal{R} = 3$ for PROTEINS. We present the average cycle length after alignment in Table 7 and the discrepancy between small and large graphs is significantly reduced.

Algorithm 2 Add One Cycle Length

```

1: procedure ADD1_CYCLE_LENGTH( $\mathcal{G}$ : input graph,  $\mathcal{C}$ : list of cycle basis)
2:   for each cycle  $\mathcal{C}_i$  do
3:     edge  $(v_1, v_2) \leftarrow \text{RandomChoice}(\mathcal{C}_i)$ 
4:      $\mathcal{G} \leftarrow \text{RemoveEdge}(v_1, v_2)$ 
5:      $v_{\text{new}} \leftarrow \text{ReplicateNode}(\arg \min_{\text{degree}}(\mathcal{C}_i))$ 
6:      $\mathcal{G} \leftarrow \text{AddNode}(v_{\text{new}})$ 
7:      $\mathcal{G} \leftarrow \text{AddEdge}(v_1, v_{\text{new}}) \text{ AddEdge}(v_2, v_{\text{new}})$ 
8:   return  $\mathcal{G}$ 

```

Algorithm 3 Align Cycle Length

```

1: procedure ALIGNCYCLELENGTH( $\{\mathcal{G}_i\}_{i=1}^N$ : a set of graphs,  $\mathcal{R}$ : skipping ratio,  $n$ : increased cycle length,  $n \geq 1$ )
2:   ResultList  $\mathcal{M} \leftarrow []$ 
3:   for  $i = 0, 1, \dots, N - 1$  do
4:      $\mathcal{G}' \leftarrow \mathcal{G}_i$ 
5:     if  $i \bmod \mathcal{R} == 0$  then
6:       for  $j = 0, 1, \dots, n - 1$  do
7:         obtain Cycle Basis  $\mathcal{C} \leftarrow \mathcal{G}'$ 
8:          $\mathcal{G}' \leftarrow \text{Add1CycleLength}(\mathcal{G}', \mathcal{C})$ 
9:      $\mathcal{M} \leftarrow \text{append } \mathcal{G}'$ 
10:  return  $\mathcal{M}$ 

```

E.2. Ablation Study on Randomly Adding Nodes

One natural question arising from Section 3.3.1 is whether the cycle length alignment is necessary or it suffices to add nodes / edges randomly in order to reduce the spectrum discrepancy between small and large graphs. To answer this question, we conduct an ablation study on adding nodes and edges randomly to the graphs in the small dataset, *matching the quantity* introduced during the cycle length alignment process. We then compare the changes in the relative spectrum difference with those observed during the cycle length alignment procedure.

We present our results in Table 8. We find that aligning cycle lengths consistently leads to smaller spectrum differences between graphs of varying sizes compared to randomly adding nodes. These results further highlight the importance of cycle lengths for GNNs to achieve size generalizability.

F. Ablation Studies on Attention Mechanism

The results in Table 9 demonstrate that +NA does not consistently enhance graph classification for large graphs. This suggests that relying solely on the attention mechanism, without considering cycle information, does not improve the size generalizability of GNNs. In contrast, the incorporation of cycle information in +SIA leads to significant improvements on large graphs.

G. Training Details

In this section, we provide the details of our training process for the purpose of reproducibility.

Size Generalization of Graph Neural Networks on Biological Data: Insights and Practices from the Spectral Perspective

Table 8. Comparison between randomly adding nodes and aligning cycle lengths. Average Wasserstein distance of eigenvalue distributions between graphs of similar size and different sizes are computed. Relative difference is computed as in Table 1. We use \uparrow (\downarrow) to denote the increase (decrease) in the relative difference compared to not taking the corresponding action. Aligning cycle lengths results in a greater reduction of the relative spectrum difference compared to randomly adding a node.

Datasets	Randomly adding nodes			Aligning cycle lengths		
	Different sizes	Similar size	Δ relative difference	Different sizes	Similar size	Δ relative difference
BBBP	0.00557	0.00203	\downarrow 33%	0.00565	0.00211	\downarrow 41%
BACE	0.00406	0.00162	\downarrow 26%	0.00417	0.00176	\downarrow 41%
NCI1	0.00559	0.00230	\downarrow 20%	0.00566	0.00242	\downarrow 31%
NCI109	0.00558	0.00232	\downarrow 22%	0.00568	0.00245	\downarrow 31%
PROTEINS	0.00756	0.00280	\downarrow 24%	0.00763	0.00302	\downarrow 41%

Table 9. Size generalizability evaluated with +NA, following the same rule as in Table 3. Naive attention is not helpful for size generalization.

Datasets	BBBP		BACE		PROTEINS		NCI1		NCI109		Avg Improv	
	Small	Large	Small	Large	Small	Large	Small	Large	Small	Large	Small	Large
MLP	90.36 \pm 0.71	55.61 \pm 3.37	61.06 \pm 5.79	21.06 \pm 7.89	36.15 \pm 2.28	21.55 \pm 1.34	36.43 \pm 3.89	3.36 \pm 2.87	35.87 \pm 4.23	4.65 \pm 3.72	-	-
MLP+NA	88.83 \pm 1.40	62.09 \pm 10.27	56.38 \pm 15.89	21.34 \pm 8.52	38.87 \pm 13.04	29.42 \pm 23.83	28.89 \pm 5.96	1.98 \pm 0.98	38.33 \pm 6.74	1.55 \pm 0.01	-1.71	+2.03
MLP+SIA	90.38 \pm 1.05	62.79 \pm 7.55	60.85 \pm 7.83	21.79 \pm 15.07	40.68 \pm 3.56	33.57 \pm 11.87	35.42 \pm 3.83	3.26 \pm 2.55	39.20 \pm 2.96	12.2 \pm 5.05	+1.33	+5.48
GCN	91.37 \pm 0.59	68.59 \pm 7.47	63.68 \pm 6.63	28.72 \pm 14.26	72.35 \pm 2.58	40.57 \pm 7.67	54.91 \pm 2.37	28.80 \pm 7.57	60.83 \pm 1.92	30.45 \pm 4.34	-	-
GCN+NA	89.45 \pm 1.65	64.38 \pm 7.10	62.03 \pm 1.12	28.19 \pm 16.32	69.95 \pm 3.27	52.41 \pm 8.71	60.37 \pm 1.40	31.52 \pm 4.18	54.97 \pm 2.57	27.60 \pm 10.07	-1.27	-0.41
GCN+SIA	91.32 \pm 0.73	71.66 \pm 6.99	64.35 \pm 9.76	24.24 \pm 17.03	73.84 \pm 3.65	58.74 \pm 9.49	59.78 \pm 1.65	45.70 \pm 6.70	60.32 \pm 2.90	38.78 \pm 4.55	+1.29	+8.40
GAT	91.27 \pm 1.43	68.35 \pm 7.02	69.73 \pm 2.05	42.23 \pm 11.18	72.25 \pm 4.25	43.86 \pm 6.82	58.22 \pm 2.86	49.36 \pm 4.12	64.39 \pm 3.29	38.36 \pm 8.93	-	-
GAT+NA	91.16 \pm 1.45	70.08 \pm 6.42	63.42 \pm 2.64	34.08 \pm 13.43	72.25 \pm 2.24	53.25 \pm 9.07	60.98 \pm 0.93	29.76 \pm 2.58	60.18 \pm 5.91	35.24 \pm 5.82	-1.57	-3.95
GAT+SIA	91.88 \pm 2.12	74.87 \pm 5.62	69.64 \pm 6.79	43.87 \pm 7.98	75.35 \pm 3.28	62.71 \pm 4.98	61.42 \pm 1.07	55.73 \pm 12.98	63.27 \pm 3.15	45.97 \pm 7.74	+1.14	+8.20
GIN	88.28 \pm 2.39	66.67 \pm 5.55	57.02 \pm 6.48	22.97 \pm 10.26	74.55 \pm 4.27	50.20 \pm 5.36	62.17 \pm 3.86	44.26 \pm 7.03	62.42 \pm 2.77	33.23 \pm 6.77	-	-
GIN+NA	89.59 \pm 2.64	69.89 \pm 12.97	55.46 \pm 10.59	18.92 \pm 15.76	73.59 \pm 4.06	54.14 \pm 8.14	61.15 \pm 4.62	35.73 \pm 9.73	61.62 \pm 3.08	32.73 \pm 8.67	-0.61	-1.18
GIN+SIA	92.70 \pm 0.45	75.99 \pm 4.74	61.30 \pm 6.77	24.42 \pm 16.37	74.88 \pm 4.24	51.36 \pm 7.76	62.83 \pm 1.07	42.82 \pm 8.92	63.00 \pm 4.24	41.65 \pm 4.19	+2.05	+3.78
FAGCN	90.58 \pm 1.72	64.93 \pm 7.62	62.96 \pm 2.12	24.65 \pm 11.71	70.03 \pm 5.20	42.34 \pm 6.61	43.51 \pm 4.29	10.16 \pm 7.80	55.78 \pm 3.5	22.65 \pm 12.87	-	-
FAGCN+NA	91.97 \pm 1.67	72.30 \pm 10.54	58.39 \pm 4.25	10.71 \pm 9.0	70.47 \pm 4.73	51.61 \pm 12.47	50.27 \pm 4.45	12.11 \pm 5.39	50.75 \pm 10.91	10.26 \pm 16.24	-0.20	-1.55
FAGCN+SIA	90.17 \pm 2.83	74.65 \pm 9.13	62.40 \pm 3.36	30.35 \pm 13.48	71.30 \pm 5.79	48.94 \pm 10.62	46.95 \pm 5.71	10.99 \pm 7.50	52.82 \pm 6.28	19.08 \pm 5.32	+0.16	+3.86
GNNML3	92.01 \pm 1.56	64.18 \pm 6.99	62.31 \pm 4.90	32.94 \pm 12.86	71.59 \pm 3.5	40.74 \pm 15.0	63.73 \pm 4.67	51.75 \pm 9.05	59.39 \pm 3.76	33.80 \pm 11.19	-	-
GNNML3+NA	87.85 \pm 1.96	66.42 \pm 1.93	65.15 \pm 7.50	42.05 \pm 13.30	66.11 \pm 10.07	55.39 \pm 13.23	59.58 \pm 5.06	32.48 \pm 8.90	60.76 \pm 4.95	27.18 \pm 8.65	-1.92	+0.02
GNNML3+SIA	92.70 \pm 0.81	70.43 \pm 6.36	64.57 \pm 2.72	37.73 \pm 7.68	69.32 \pm 3.79	48.94 \pm 10.62	63.91 \pm 5.81	48.85 \pm 12.11	61.58 \pm 3.98	49.70 \pm 17.85	+0.61	+6.45

To ensure fair comparisons, we maintain consistent hyperparameter settings across all experiments. Specifically, we use a batch size of 30 and a learning rate of 0.001. The Adam optimizer is employed without gradient clipping. For the baseline models, we utilize three graph convolution layers with a global max pooling. The previously described upsampling technique is applied to all methods. To prevent overfitting, we implement early stopping with a patience period of 50 epochs, and the lowest validation loss as the criterion for model selection. Each method is executed five times, and we report the average result along with the standard deviation in Table 3 and Table 4.

To ensure consistency with the original papers, we set the other hyperparameters of each baseline model to match the values specified in their respective papers. For +SSR, we use the same hyperparameter settings as in (Buffelli et al., 2022) and set the regularization coefficient $\lambda = 0.1$ and coarsening ratios $C = \{0.8, 0.9\}$ for all datasets. We adhere to the authors’ recommendation and employ spectral graph coarsening as the coarsening algorithm. Additionally, we fine-tune the aggregation strategy, selecting from options such as max, mean, and sum, to derive features for the nodes in the coarsened version. For SMP and +RPGNN, we use the original code provided by the authors. For SMP, we tune the number of SMP and FastSMP layers from the set $\{3,4\}$. Based on the validation results, we implement 3 FastSMP layers. For +RPGNN, we use the same hyperparameter settings as in (Bevilacqua et al., 2021; Buffelli et al., 2022). For +CIGA, we follow the same hyperparameter search range as specified in (Chen et al., 2022). Regarding the +SSL method that we proposed, we tune λ over $\{1, 1e - 1, 1e - 2, 1e - 3, 1e - 4, 1e - 5\}$. Based on the validation results, we identify $\lambda = 1e - 2$ for NCI1, and NCI109, $\lambda = 1$ for PROTEINS, BBBP, and $\lambda = 1e - 2$ for BACE. For our proposed cycle augmentation, we use the set of hyperparameters n, \mathcal{R} from Appendix E.1. For +SIA, we have no hyperparameters to tune.

Table 10. Average Wasserstein distance between graphs of ‘similar sizes’ and graphs of ‘different sizes’ based on **degree** distributions, respectively. The relative difference is computed by the difference of the Wasserstein distance normalized by the Wasserstein distance of similar graphs.

	BBBP	BACE	PROTEINS	NCI109	NCI1
Different Size	0.00177	0.00120	0.00062	0.00161	0.00163
Similar Size	0.00157	0.00105	0.00054	0.00146	0.00148
Relative Difference	12.1%	14.6%	14.8%	10.1%	9.8%

H. Additional Plots on Degree Distributions

Figure 3 and Table 10 reveal that the degree distribution does not exhibit a clear correlation with the graph size. These visualizations and tables adhere to the same convention as presented in Section 3.2. Unlike the assumption made in (Yehudai et al., 2021) that attributes changes in local degree patterns as the primary covariate shifts induced by size, our investigation on biological datasets suggests a different perspective.

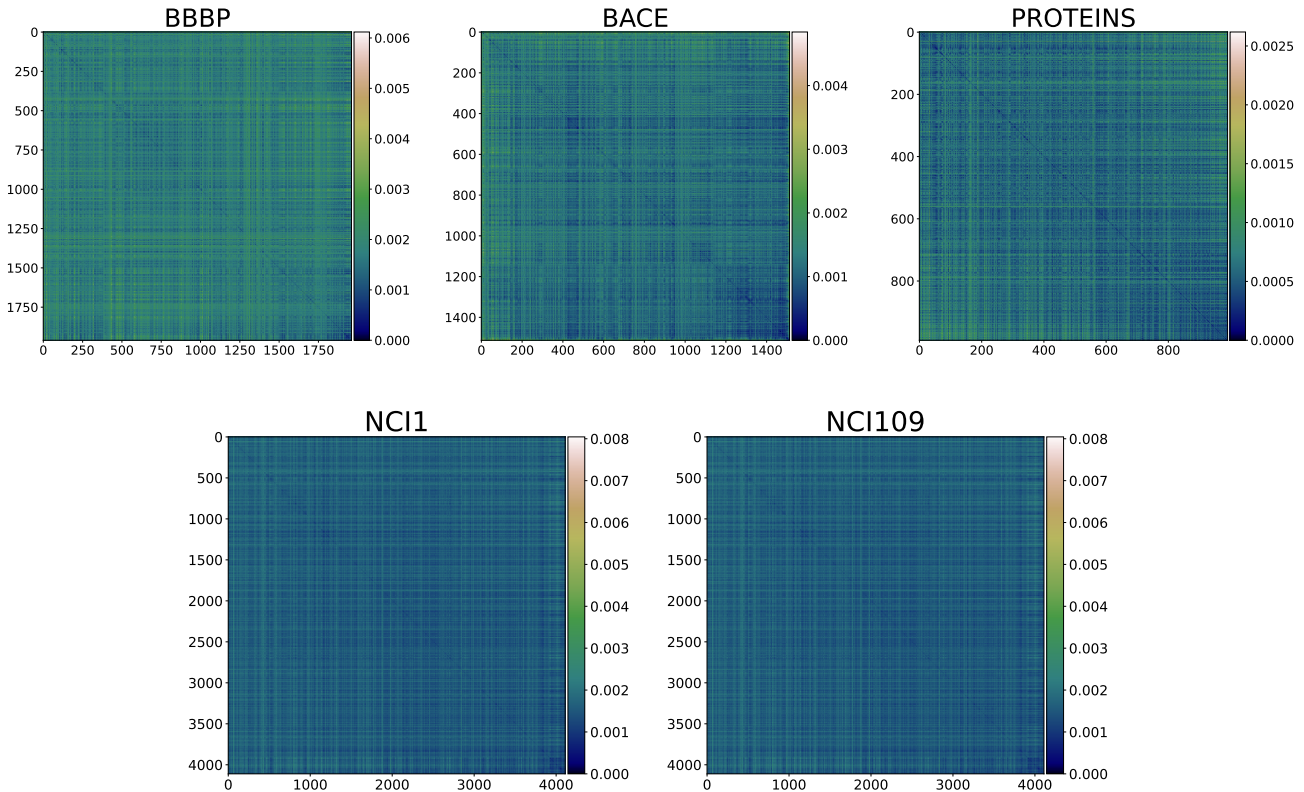


Figure 3. Pairwise graph distance measured by the Wasserstein distance of degree distributions, following the same convention in Figure 1. **Degree distribution does not show a clear correlation with graph size.**

I. Additional Results on Real-world Datasets

In this section, we demonstrate +SIA’s effectiveness in size generalization using the HIV dataset from (Hu et al., 2020a). Adopting the ROC-AUC metric from (Chen et al., 2022; Hu et al., 2020a), we observe that +SIA still consistently achieves performance improvements across all backbone models.

Table 11. Size generalizability evaluated on the real-world hiv datasets. +SIA still leads to consistent performance boosts.

Dataset	Hiv											
Models	MLP		GCN		GAT		GIN		FAGCN		GNNML3	
	Small	Large	Small	Large	Small	Large	Small	Large	Small	Large	Small	Large
Original Performance	67.95±2.22	38.97±6.39	71.29±1.58	38.35±4.09	73.34±1.77	41.23±4.62	71.04±1.45	43.65±3.01	68.35±3.09	50.03±1.85	74.32±1.13	47.44±7.66
+SIA Performance	70.64±1.94	40.93±2.87	70.27±1.42	43.24±6.08	72.33±1.72	46.72±2.74	69.92±1.50	43.55±3.84	69.53±1.92	52.35±6.35	74.52±2.95	54.68±6.60
+Avg Improvements	(small) +0.15 ; (large) +3.63											

J. Additional Plots on Cycle Breaking & Cycle Length Alignment

Following the same convention in Figure 2, Figure 4 presents the pairwise graph distance measured by eigenvalue distributions after breaking cycles and aligning cycles on other datasets.

K. Limitations of d-Patterns in Capturing Cycle Information

In this section, we show that the challenges identified in our findings cannot be addressed by the previous work (Yehudai et al., 2021). Yehudai et al. (2021) introduce the concept of “d-patterns” to characterize the information learned by GNNs for each node. It demonstrates that the presence of unseen d-patterns in large test graphs results in significant test errors for GNNs. We first begin with their definition:

Definition K.1 (d-pattern (Yehudai et al., 2021)). Let C be a finite set of node features, and let $G = (V, E)$ be a graph with node feature $c_v \in C$ for every node $v \in V$. We define the **d-pattern** of a node $v \in V$ for $d \geq 0$ recursively: For $d = 0$, the 0-pattern is c_v . For $d > 0$, the d -pattern of v is $p = (p_v, \{(p_{i_1}, m_{i_1}), \dots, (p_{i_l}, m_{i_l})\})$ iff node v has $(d - 1)$ -pattern p_v and for every $j \in \{1, \dots, l\}$ the number of neighbors of v with $(d - 1)$ -patterns p_{i_j} is exactly $m_{p_{i_j}}$. Here, i is the number of distinct neighboring $d - 1$ patterns of v .

The notion of d-patterns highly resembles the idea of the 1-Weisfeiler-Lehman algorithm and suffers from the same limitations in differentiating cycles. In the following lemma, we show that the d-patterns for every node in the featureless cycle graphs of varying sizes are identical.

Lemma K.2. Consider a set of distinct cycle graphs $\{\mathcal{G}_n = (V_n, E_n)\}_{n=1}^k$, where each graph \mathcal{G}_n in the set has a unique number of vertices n with $n \geq 3$ and has no node features, then the d -pattern of each node is identical for all graphs. i.e. $d\text{-pattern}(v_i) = d\text{-pattern}(v_j) \forall v_i, v_j \in V_n, \forall n$.

Proof. We can prove this statement through induction on d . The 1-pattern corresponds to the node’s degree. In any cycle graph, the degree of any node is the same, which equals 2. For induction, we assume the statement holds for k -pattern, i.e. the k -pattern of every node is \mathcal{K} . Then we aim to prove the statement for the $(k + 1)$ -pattern. Note that every node has two neighboring nodes. By the recursive update rule of d -pattern, the $(k + 1)$ -pattern of any node is $(\mathcal{K}, \{(\mathcal{K}, \mathcal{K})\})$ and thus the $(k + 1)$ -pattern of every node is identical. \square

The above lemma points out that d-patterns cannot distinguish nodes in cycles of varying sizes, suggesting that our study of cycles is orthogonal to the study in (Yehudai et al., 2021).

Furthermore, suffering from the same limitation as 1-WL, d-patterns would produce identical embeddings for some pairs of non-isomorphic graphs containing cycles with node features, as can be seen in Figure 5 and proved in Claim K.3. Moreover, d-pattern can fail to distinguish graphs that 1-WL cannot distinguish, with abundant existing counter-examples in existing literature. This essentially implies that d-patterns that are seen during training time, may comprise different graphs during test times and thus contradict previous conclusions. Those corner cases usually involve cycles. Thus, cycle information should be treated independently in the problem of GNN size generalization.

Claim K.3. The d -pattern of each node with the same id in Figure 5 is identical.

Proof. We can prove this statement through induction on d . The statement can be easily verified for $d = 0$ or 1. Suppose the statement holds for $d \leq k$ and we want to show that it holds for the $(k + 1)$ -pattern. Note that the statement naturally holds for node 0, 4 since their $(k + 1)$ -pattern is dependent on the k -pattern of the same neighbor nodes. WLOG it suffices to consider the $k + 1$ -pattern node 2 for the rest of the cases, where we can enumerate all the recursive update cases from

Figure 6. It is clear to observe that in each hierarchy the dependent neighbor patterns are the same and thus the d-pattern is identical. Hence we prove this claim.

□

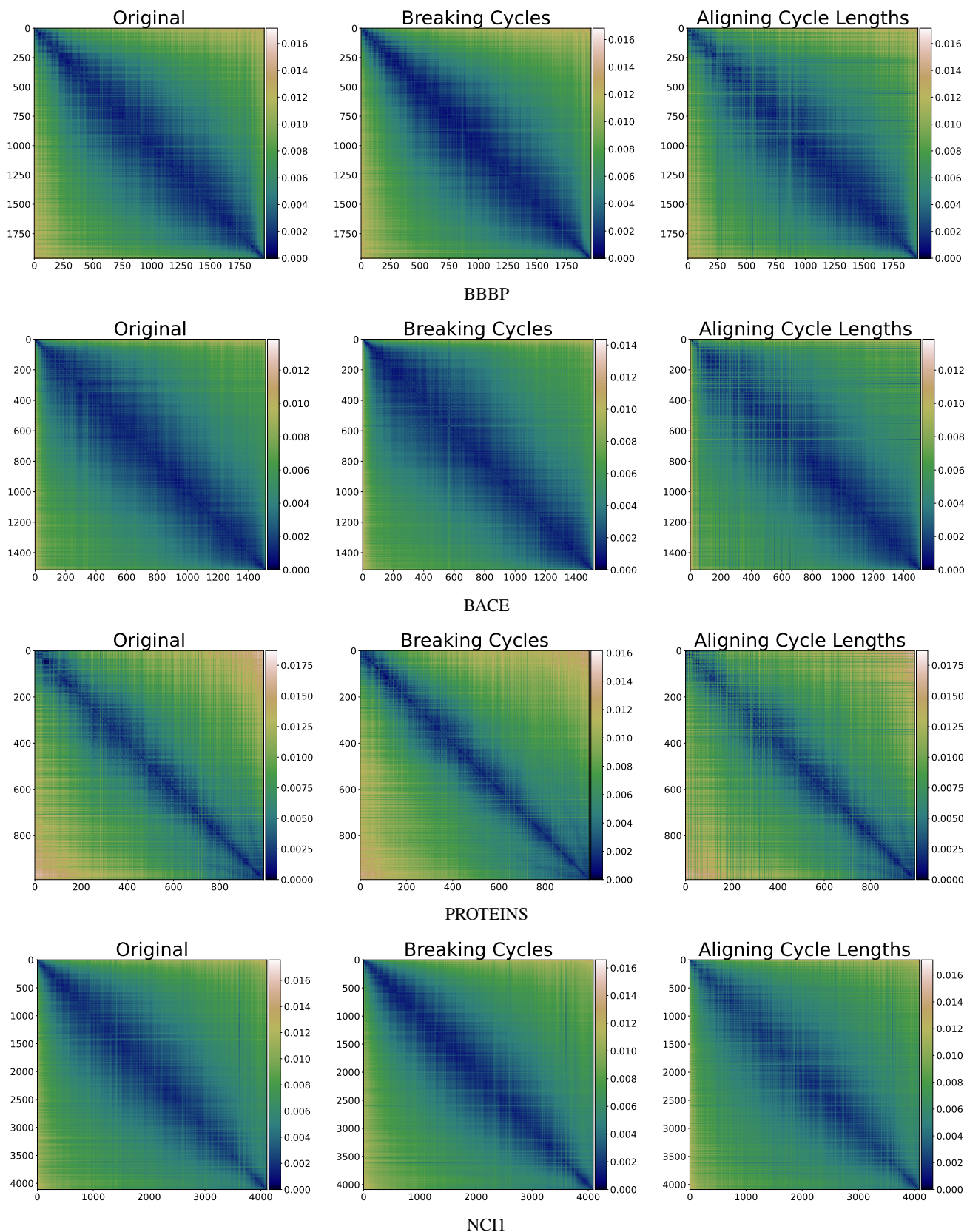


Figure 4. Pairwise graph distance measured by the Wasserstein distance of eigenvalue distributions after breaking cycles and aligning cycle lengths on different datasets. Breaking cycles **amplifies the correlation** between eigenvalue distribution and graph size, while aligning cycle lengths **reduces the correlation**.

